Radiation induced solute clustering in high-Ni reactor pressure vessel steel

M.J. Konstantinović, I. Uytdenhouwen, G. Bonny, N. Castin,

Studiecentrum voor Kernenergie/Centre d'Etude de l'Energie Nucléaire, SCK·CEN, Boeretang 200, 2400 Mol, Belgium

L. Malerba

Centro de Investigaciones Energéticas, Medioambientales y Tecnológicas, CIEMAT, Edificio 30 - E30 P0.13, Avda Complutense 40, 28040 Madrid, Spain

P. Efsing

Vattenfall Ringhals AB, Väröbacka SE 430 22, Sweden

Abstract

The thermal stability and the structure of solute-vacancy clusters formed by neutron irradiation are studied by means of positron annihilation spectroscopy and hardness measurements of post-irradiation annealed reactor pressure vessel steels with high and low Ni contents. Two distinct recovery stages were observed and assigned to (a) the dissolution of vacancy clusters at about 650 K, and (b) the dissolution of solute-vacancy clusters at about 750 K. In steels with high Ni content, hardening mainly recovers during the second stage. Atomistic and coarse grain models suggest that during this stage, the removal of vacancies from vacancy-solute clusters leads to complete cluster dissolution, which indicates that solute clusters are radiation induced.x

Keywords: vacancy-solute clusters, neutron irradiation, positron annihilation, high Ni RPV steel

*Corresponding author
Email address: mkonstan@sckcen.be (M.J. Konstantinović)

Preprint accepted for publication in Acta Materialia

1. Introduction

RPV steels are exposed to non-equilibrium thermodynamic condition created by energetic neutron bombardment during nuclear power plant operation. Abundance of vacancies and self-interstitials formed under these conditions may induce migration of alloying elements and formation of complex defects such as solute-rich clusters. Solute-rich clusters, or precipitates formed under neutron irradiation, are known to be the cause of hardening and subsequent embrittlement of RPV steels. Even though of nanometric size, these clusters or precipitates strongly affect the motion of dislocations, causing macroscopic changes in mechanical properties [1, 2]. In order to predict the kinetics of hardening and embrittlement versus neutron dose and to assess the hardening effect of solute clusters or precipitates it is crucial to understand the underlying process of formation, in particular it is important to determine whether they are real precipitates or complexes containing solutes and point-defects, stabilized by the presence of the latter. Numerous studies based on the atom probe tomography (APT) [3, 4, 5, 6, 7] have shown that under irradiation most major solute atoms in RPV steels cluster together. The main contribution to hardening comes from copper-rich precipitates of a few nanometers in diameter, which are easily formed under neutron irradiation due to the low solubility of Cu in Fe. The easy formation of Cu-rich clusters is reflected by (a) their appearance at relatively low fluence, and (b) the fact that their formation is expected based on FeCu binary phase diagram. Still, there is another class of RPV steels with high Ni and Mn content and virtually no Cu, which exhibit substantial hardening and embrittlement under neutron irradiation. This cannot be assigned to Cu-rich precipitates. An example is the steel used to fabricate the vessel of a number of power plants in Sweden, at the Ringhals site (Ringhals steels). In this class of steels, APT revealed the existence of a large volume fraction of Ni-Mn rich clusters [8], (the composition of which does not match the composition of any thermodynamically expected phase) [9, 10]. It is important to mention that APT also revealed the existence of a population of Ni-Mn rich clusters in the

16MND5 RPV steel, which has a lower Ni content, and consequently, the volume fraction of solute clusters is lower and the materials exhibits lower hardening in comparison with Ringhals steels [11]. Because of the non-applicability of a thermodynamic approach under non-equilibrium conditions, the formation and stability of the Ni-rich clusters are not yet fully understood [2]. As APT cannot detect lattice defects, the role of point-defect such as vacancies, in particular their presence in association with solute clusters, remains to be investigated in more depth. In our previous study the properties of vacancy-solute clusters were analyzed based on positron annihilation experiments in post-irradiation annealed FeCu, FeMnNi, and FeCuMnNi alloys [12]. From the comparison between the experiments and rigid lattice calculations, the existence of vacancy clusters enriched with Ni and Mn with significantly higher thermal stability and larger dissociation energy than all other small vacancy(-solute) clusters was deduced. The present study significantly extends the previous by investigating the properties of solute-vacancy clusters in RPV steels with low and high Ni content. Extending the study to actual steels is crucial, because even though model alloys may help understand mechanisms, the quantitative results obtained from them may be misleading. For instance, if conclusions on the behavior of 16MND5 had to be drawn based on the FeCuMnNi model alloy analyzed in our previous work, where the Cu, Mn and Ni contents are very similar to those of those of the steels, one should conclude that vacancies must be present also in the solute clusters that formed in the steel. This paper shows that such conclusion would not be correct and that the complexity of steels requires higher Ni contents to see similar effects.

2. Materials and experiments

The materials used in this study are two RPV steels with high and low Ni contents. The chemical composition of the investigated RPV steels is given in Table 1. Low Ni, 16MND5 steel samples were neutron irradiated in the Belgian Reactor (BR2) up to 0.1 *displacement per atom*, *dpa*, $(6.9 \times 10^{19} n/cm^2)$, at the

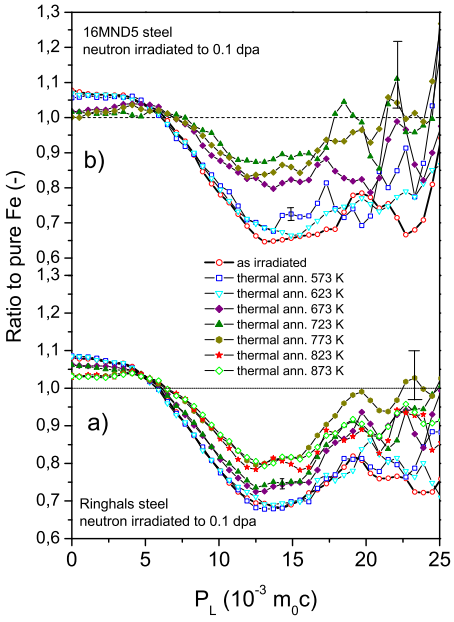

Figure 1: (Color online) Doppler broadening spectra of the a) Ringhals, and b) 16MND5 steels. Measurement error increases with P_L; minimum and maximum values are shown.

Table 1: The nominal composition of Ringhals and 16MND5 RPV steels. Fe is the balance.

Material comp.(wt.%)	C	Si	Mn	P	S	Cr	Mo	Ni	Cu	V	Co	A
Ringhals	0.052	0.21	1.46	0.009	0.006	0.07	0.54	1.58	0.08	0.002	0.015	0.0
16MND5	0.16	0.19	1.35	0.006	0.005	0.18	0.51	0.74	0.07	-	0.01	

temperature and pressure of about 300 $^{\circ}C$ and 150 bar, respectively [13]. Two Ringhals steel samples (weld), Ringhals96 and Ringhals93, with high Ni content were extracted from the surveillance specimens [10] which were irradiated at the temperature of 284 $^{\circ}C$, reaching the fluence of $6.87 \times 10^{19} n/cm^2$ and $5.18 \times 10^{19} n/cm^2$, respectively.

Post-irradiation isochronal annealing (0.5 h) experiments were performed at various temperatures in the range between 573 K and 923 K (300 to 650 ^{0}C). The same set of samples (two for PAS and one for hardness per material) were simultaneously annealed and used in the whole temperature range.

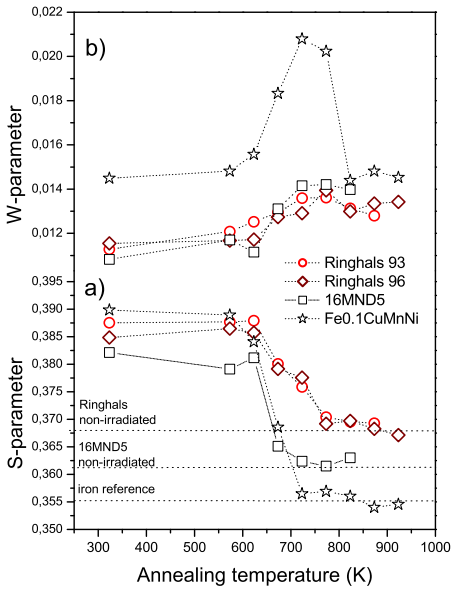

Figure 2: (Color online) a) S and b) W parameters versus the annealing temperature

PAS experiments were performed with the Coincidence Doppler broadening spectrometer (CDB) and positron annihilation lifetime spectrometers (PALS). The CDB spectra were measured using two Ge detectors. Details of the setup are described in [14]. The CDB spectrum provides the momentum distribution of the core electrons, which can be used to determine the chemical environment of a positron-electron annihilation site [15]. The PALS measurements, which provide the size and density of vacancy type defects, were performed with a spectrometer working in a triple coincidence mode with a time resolution of about 175 ps. The triple coincidence mode is used for irradiated materials in order to reduce the background originating from γ rays of the radioactive samples.

Hardness of the samples was measured with Vickers micro-hardness set-up, Reichert-Jung Micro-duromat 4000E mounted on a nuclearized Leica Telatom 3 optical microscope.

3. Computation methods

The dissociation energy of a vacancy from a vacancy-solute cluster (VSC), $E_{\mathrm{dis}} = E_{\mathrm{b}} + E_{\mathrm{m}}$, was calculated using a rigid lattice model in the standard approximation [16], as the sum of the binding energy of a single vacancy, v, to a VSC, $E_{\mathrm{b}}(v_m S_n) = E(v_{m-1} S_n) + E(v) - E(v_m S_n) - E(Fe)$, and the vacancy migration energy in *bcc* Fe. The latter was taken to be E_m=0.70 eV, following density function theory (DFT) data [18, 17]. The $E(v_{m-1} S_n)$ and $E(v_m S_n)$ denote the total energy containing a $v_{m-1} S_n$ and $v_m S_n$ cluster, respectively. $E(v)$ is the total energy containing one vacancy, and $E(Fe)$ is the total energy of the perfect Fe crystal.

The rigid lattice model is based on a cluster expansion including triplet interactions up to the second nearest neighbour distances [19]. Amongst other data, the cluster expansion was fitted to reproduce the DFT energetics of small vacancy-solute clusters [19]. The latter model presents an improved description compared to the pair interaction model from [20], that was used in our previous work [12].

The calculations were performed in the periodic body centered cubic *bcc* crystals containing 1024 atoms, which proved sufficient to remove any box size effect. The VSCs were constructed in the most compact way such that the vacancy cluster is at the center of the VSC. The investigated VSCs had a diameter of about 1.4 nm, consistent with APT observations, and contained 1-6 vacancies. The solute concentration in the VSC was chosen consistent to APT observations for Ringhals steels [9], i.e., 50% Fe, 25% Ni and 25% Mn. Minor solute elements including Cu were neglected. To sample the distribution function in E_{b}, the same composition was sampled 1000 times.

The simulation of post-irradiation annealing experiment was performed using the object kinetic Monte Carlo (OKMC) technique. Two defects populations were defined: (A) pure vacancy clusters; (B) solute decorated vacancy clusters. The proportionality between both populations is characterized by the fraction x_{VSC}, representing the fraction of VSC over the total number of vacancy(solute)

clusters. It is worth noting that this proportion describes the initial state only, while the system spontaneously reconfigures during the post-irradiation annealing. A dissociation energy is defined for the event of emission of a single vacancy out of a cluster. These are denoted as E_v and $E_{\mathrm{VSC}} > E_v$, in the undecorated and decorated cases, respectively. A migration event is defined for single vacancies, with a migration energy of $0.70eV$. The initial state is taken in such a way that the vacancy concentration is $10^{25}m^{-3}$, distributed in clusters whose size follows a Gaussian distribution with average 5 vacancies, and a variance of 3 vacancies. Vacancies are eliminated from the system assuming a sink strength equivalent to the dislocation density ($10^{14}m^{-2}$) and grain size ($\sim 1\mu m$) of the material. The temperature is gradually increased respecting the specifications of the experimental post irradiation annealing performed in this work. The output of the OKMC model is compared to the PAS-CDB data, by normalizing the initial concentration of vacancies to unity, as well as the initial value for the S-parameter.

4. Results and discussion

4.1. Positron annihilation spectroscopy

The CDB spectra of Ringhals and 16MND5 steels annealed at various temperatures are shown in Fig.1 a) and (b), respectively. Both steels have strong enhancement in the low momentum region, indicating that positrons are trapped and annihilate in the open volume defects induced by irradiation such as vacancies and voids. In the high momentum region, Fig.1 very small difference between Ringhals and 16MND5 steels was observed, see more discussion below. By increasing the annealing temperature, the CDB spectra of two steels gradually change, with a tendency to reach the CDB spectra of non-irradiated steels. No significant change of the CDB spectra was found in Ringhals and 16MND5 steels at temperatures above 823 and 723 K, respectively. At these temperatures, the difference between the CDB spectra of thermally annealed steels and the reference spectrum (pure Fe) is assigned to initial steel conditions. Both

steels show more open volume defects in non-irradiated state than in pure Fe (reference), mainly due to dislocations.

CDB spectra, i.e. the low and high-momentum regions can be quantified based on the S- and W-parameters, respectively. The S- and W-parameters are defined as the ratio of low momentum ($|p_L| < 2.5 \times 10^{-3}\,\mathrm{m_0c}$) and high momentum ($15 \times 10^{-3}\,\mathrm{m_0c} < |p_L| < 25 \times 10^{-3}\,\mathrm{m_0c}$) regions of the Doppler broadening spectra to the total momentum, respectively. The S- and W-parameters versus the annealing temperature are presented for the two steels in Fig.2 a) and b). The increase of the annealing temperature causes the decrease of the S-parameter (low-momentum contribution) in all samples, as a consequence of the dissociation/dissolution of vacancy complexes. Interestingly, in both Ringhals samples the decrease of the S-parameter occurs in a broader temperature interval in comparison with the 16MND5 steel sample, see Fig.2 a). In fact, two annealing stages at the temperatures of about 650 and 750 K can be resolved. Both annealing stages agree very well with previously observed annealing stages of neutron irradiated FeCu, FeCuMnNi and FeMnNi alloys [12]. Namely, the first annealing stage at about 650 K corresponds to the dissolution of vacancy clusters, while the second annealing stage at about 750 K is assigned to the dissolution of vacancy-Ni rich solute complexes [12]. In Ringhals steel, the second annealing stage is found to be more pronounced than in the model alloys. As discussed later on, its enhancement in Ringhals steel can be ascribed due to the higher Ni content of the Ringhals steel as compared to model alloys.

In Ringhals steel, the W-parameter exhibits a weak peak at the temperature of about 800 K. The peak in the W-parameter typically indicates the existence of Cu-rich precipitates, which were formed under neutron irradiation [21, 13, 22]. According to previous studies, the peak position of the W-parameter can be correlated to the concentration of copper and corresponding Cu solubility limit (i.e. FeCu phase diagram) [12]. Since the peak position of the W-parameter in Ringhals steel is found to be very close to the peak position of W-parameter in FeCuMnNi, see Fig.2b), both Ringhals steel and FeCuMnNi alloy should have similar Cu concentration. This is indeed the case, both materials have Cu

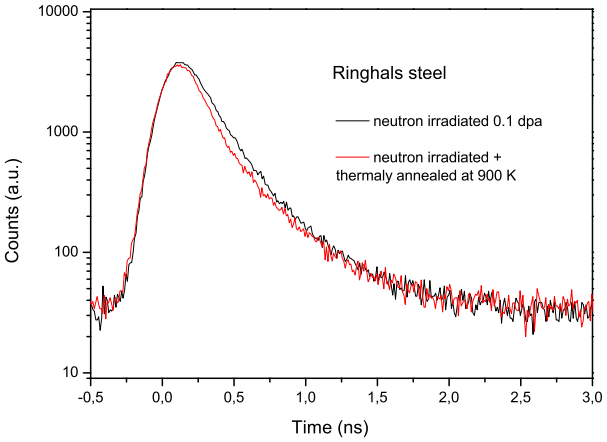

Figure 3: (Color online) Lifetime spectra of irradiated and post irradiated thermally annealed Ringhals steels.

content close to 0.1 wt %, see Table 1 and Ref. [12].

The PALS spectra of neutron irradiated and post neutron irradiated thermally annealed Ringhals steel are shown in Fig.3. The spectra were analyzed by assuming the existence of two positron lifetime components. The PALS spectra of 16MND5 steel were analyzed only with one lifetime component, because no significant improvement of the fit could be reached with two lifetime components analysis. The effect of vacancy cluster annealing is clearly seen by the reduction of the long positron lifetime component. The short lifetime component is estimated to be of about 100 ps, which is close to the value in bulk Fe. All lifetime components as a function of the annealing temperature are presented in Fig.4. Interestingly, the long lifetime component in neutron irradiated Ringhals steel samples prior to thermal annealing was found to be about 225 ps and 255 ps with an intensity of about 50 % and 30 % for Ringhals93 and 96, respectively. These values indicate that vacancy clusters formed in neutron irradiated Ringhals steels contain about 5-6 vacancies in average. This is in clear contrast with the result in the 16MND5 steel where this value is close to that of a monovacancy. Furthermore, the average lifetime component of both Ringhals steel samples decreases by increasing the annealing temperature, which correlates

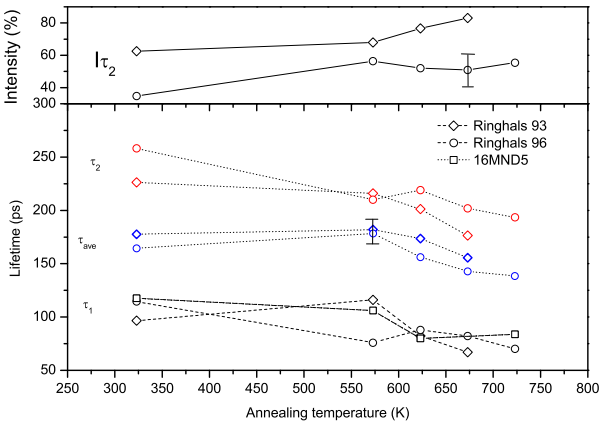

Figure 4: PALS lifetime of Ringhals and 16 MND5 steels versus annealing temperature.

nicely with a decrease of the S-parameter obtained from Doppler broadening spectra.

4.2. Computation

To rationalize the different annealing stages in S-parameter between 16MND5 and the Ringhals steels, we performed OKMC simulation to calculate the dissolution of different vacancy-rich clusters. Starting from a single population of vacancy-rich cluster, the evolution of the S-parameter for the 16MND5 steel is best reproduced for $E_v = 1.1eV$, as shown in Fig. 5. However, the second annealing stage observed in Ringhals steels was impossible to reproduce employing a single cluster population.

Therefore we introduced a second vacancy-rich population with fraction x_{VSC} and different dissociation energy E_{VSC}. We found that $x_{\mathrm{VSC}} = 0.04$ and $E_{\mathrm{VSC}} = 1.3eV$ reproduces the evolution of the S paramter for Ringhals steels the best. A comparison between the simulation results and the renormalized CDB data is presented in Fig. 5. Thus, the simulations show that the experimental data can be interpreted as the dissolution of two different populations of vacancy-rich clusters with a relative difference in dissociation energy of 0.2 eV.

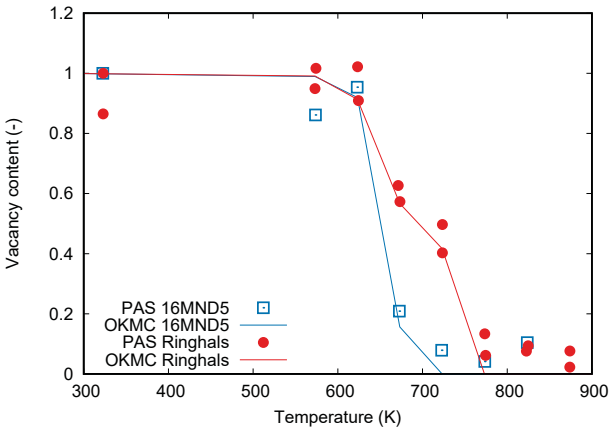

Figure 5: (Color online) Comparison of the predicted vacancy content in the 16MND5 and Ringhals steels following the OKMC model with the corresponding rescaled S-parameters.

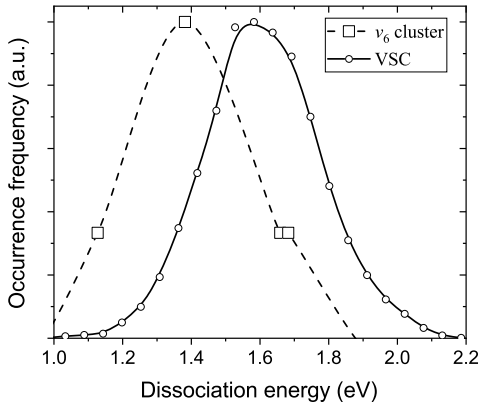

Figure 6: Occurrence frequency in arbitrary units of the binding energy of a vacancy to a pure vacancy cluster (dotted line) and to VSC (full line) containing 6 vacancies.

In an effort to characterize these two different vacancy-rich cluster populations, we performed atomistic simulations. The binding energy of a v to a pure vacancy cluster and VSC is evaluated using the rigid lattice model. Compact clusters containing 1-6 vacancies were investigated, consistent with PAS-lifetime observations. VSCs with a diameter of 1.4 nm and compact vacancy cluster at its center (1-6 vacancies) were also investigated. The VSC composition was chosen at 50% Fe, 25% Ni and 25% Mn. These cluster sizes and compositions are consistent with APT observations in Ringhals steel [9]. Maximum probability for the binding energy increases with increasing vacancy number 1-4, and then saturates for clusters containing 5-6 vacancies, for both pure vacancy and VSC clusters. The results of the calculations for 6 vacancies are presented in Fig. 6, showing the distribution of the dissociation energy of a v to a vacancy cluster and to a VSC in bcc Fe. Both curves were renormalized to yield the same maximum, which facilitates comparison. Interestingly, the difference between pure vacancy clusters and those containing solutes is about 0.2 eV. As the average vacancy number in the clusters was measured to be 5-6 vacancies, the dissociation energy of these type of clusters will dominate the annealing stages, which is exactly the difference in dissociation energy necessary to reproduce the experimental annealing stages. However the binding energy is respectively 1.4 and 1.6 eV, thus 0.3 eV higher than the values that fitted the recovery stages in OKMC. This could be an entropic effect, e.g. the formation energy of the vacancy in Fe decreases from 2.2 eV to about 1.6-1.7 at high T because of entropy, thus a similar reason could explain this shift. Vibrational entropy is obviously not included in the rigid lattice model.

Thus, the atomistic simulations confirm that the lowest annealing stage is related to the dissolution of pure vacancy clusters, while the higher annealing stage is related to the dissolutions VSC. This conclusion is consistent with our previous work [12], although the analysis there was less rigorous.

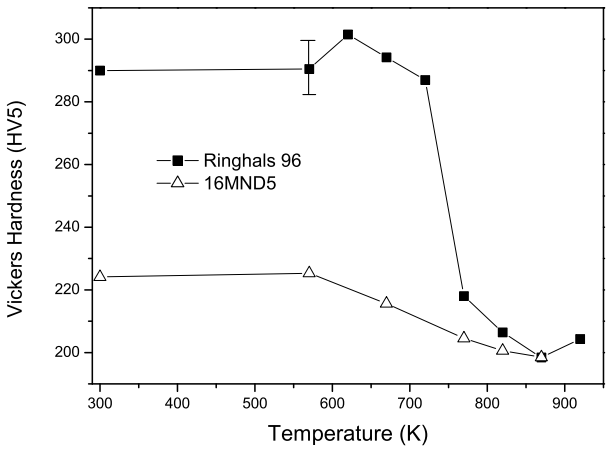

Figure 7: Vickers hardness of Ringhals and 16 MND5 steels versus annealing temperature.

4.3. Hardness

The results of hardness measurements are presented in Fig.7. As irradiated Ringhals and 16MND5 steels have Vickers hardness of about 290 and 225 HV5, respectively. The much larger hardness of the Ringhals steel is consistent with previous work [10]. By increasing the temperature, the Vickers hardness of both steels decreases towards the non-irradiated value, due to removal of defects by annealing. Interestingly, the Vickers hardness of the Ringhals steel exhibits an abrupt decrease at the temperature of 723 K. This temperature corresponds well to the second annealing stage observed by the Doppler broadening experiment, which corresponds to the dissolution of vacancy-Ni rich clusters. The fact that the mechanical property recovers at this stage points to the important role played by vacancies in the thermal stabilization of Ni-rich clusters.

4.4. Discussion

The average vacancy cluster size in Ringhals steels (5-6 vacancies in a cluster) obtained by lifetime measurements is similar to the average vacancy cluster size in high-Cu Doel steels [6] irradiated to similar dose. The presence of a similar amount of vacancies in Cu-rich and Ni-rich precipitates suggests that in both cases point-defects have a role in the nucleation and growth of solute clusters and

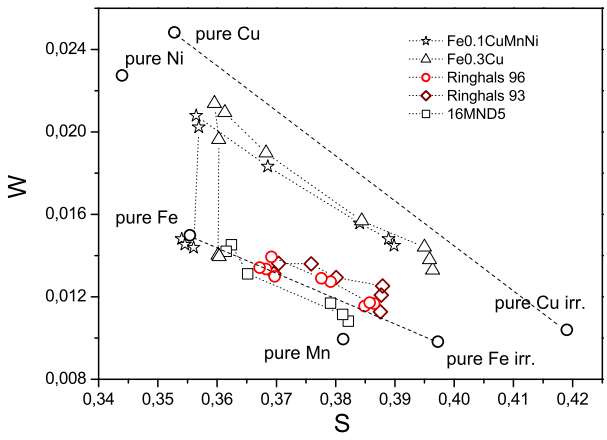

Figure 8: (Color online) W versus S for various post irradiation annealed alloys and steels.

are associated with them. There is, however, an important difference between the two cases. In the case of the Cu-rich clusters, the dissolution of vacancy clusters associated with them does not lead to the dissolution of the solute clusters, which disappear at higher temperature. The hardness drop occurs in correspondence with the disappearance of the Cu-rich clusters [23]. This indicates that Cu-rich clusters are thermodynamically stable phases responsible for hardening and that vacancies have an affinity for them, but are not needed to stabilize them. In contrast, in the case of Ni-rich clusters the removal of the vacancies determines the disappearance of the solute clusters and the hardness drop as well. This indicates that the Ni-rich, and vacancy-containing, clusters are responsible for the hardening, like the Cu-rich clusters, but vacancies are in this case essential to stabilize the clusters. Thus Ni-rich clusters are not thermodynamically stable phases, but rather radiation-induced features.

Moreover, no strong enhancement of the W-parameter due to Ni-clustering was detected by PAS experiments in irradiated Ringhals steel, even tough it is expected according to the results in non-irradiated pure Fe and pure Ni specimens. This could be the consequence of the fact that Ni-rich clusters formed in Ringhals steel have diffuse character, being rich in Fe, which would strongly reduce the signal in the high momentum region of the Doppler broadening spec-

tra. APT results of the Ringhals steel and other high Ni steels indeed revealed diffuse character of Ni-rich clusters [9, 10]. Following a diffuse cluster scenario, the cluster composition, namely their Cu content, was estimated based on W versus S plot. The plot showing the W-parameter versus the S-parameter of post-irradiation thermally annealed Ringhals and 16MND5 steels, together with Fe0.3Cu and Fe0.1CuMnNi alloys are presented in Fig.8. This graph illustrates the evolution of solute clusters as a function of the annealing temperature, and can be used to estimate the Cu content in the cluster. In FeCu binary alloys, the decrease of the S-parameter and accompanied increase of the W-parameter follow the path determined by the straight line which connects pure Cu and neutron irradiated Cu, see Fig.8. This indicates that positrons preferentially annihilate in the vicinity of Cu clusters which were formed by neutron irradiation. If there were no solute clusters formed under neutron irradiation, or no Cu atoms in the cluster (e.g. FeMnNi alloy - not shown for clarity), the S versus W dependence would follow the path that corresponds to pure Fe. The annealing path observed for Ringhals steel samples lay well below the path of FeCu binary alloy and slightly above the path of pure Fe, suggesting that a relatively small number of copper atoms are contained within the solute clusters. From the relative position of the annealing path of the Ringhals steel with respect to those of binary FeCu and pure Fe, the copper content within the solute clusters was estimated to be of about 10 %. This result is in very good agreement with the estimate based on the APT data [9].

5. Conclusion

- PAS experiments detect vacancy-rich clusters containing 5-6 vacancies on average in irradiated Ringhals steels. PAS experiments detect mono vacancy signal in 16MND5.
- Post-irradiation annealing reveals a recovery stage at 650 K in all steels and additional recovery annealing stage at 750 K for Ringhals steels.

- OKMC simulations show that these annealing stages correspond to the dissolution of two different populations of vacancy-rich clusters, with a difference in dissociation energy of 0.2 eV. The relative fraction of both cluster populations is $\sim 4\%$.
- Atomistic simulations show a difference in dissociation energy of ~ 0.2 eV for pure vacancy clusters and VSC clusters, respectively, containing 5-6 vacancies.
- Analysis of the S versus W parameter plot confirms the presence of Ni in at least part of the vacancy clusters.
- All these observations support the hypothesis that the two annealing stages correspond to the dissolution of vacancy and solute-vacancy clusters, respectively.
- The evolution of the Vickers hardness with annealing temperature shows that the dissolution of solute-vacancy clusters has a significant impact on the mechanical properties of the steel.
- Irradiation induced Ni-rich clusters do not seem to be a thermodynamically stable phase because they are thermally stabilized through interactions with small vacancy clusters.

Acknowledgments. We would like to thank J. L. Puzzolante for the support of hardness measurements. Part of this research was carried out in the frame of the EU funded project SOTERIA. Grant agreement number: 661913.

References

[1] S. B. Fisher, J. E. Harbottle, N. Aldridge, Radiation hardening in magnox pressure-vessel steels, Phil. Trans. R Soc. Lond. A 315 (1985) 301-332.

[2] Odette GR, Lucas GE, Recent Progress in Understanding. Reactor Pressure Vessel Steel Embrittlement, Radiat. Eff. Def. Solids 144 (1998) 189-231.

[3] R. G. Carter, N. Soneda, K. Dohi, J. M. Hyde, C. A. English and W. L. Server, Microstructural characterization of irradiation-induced Cu-enriched clusters in reactr pressure vessel steels, J. Nucl. Mater. 298 (2001) 211-224.

[4] M. K. Miller and K. F. Russell, Embrittlement of RPV steels: An atom probe tomography perspective, J. Nucl. Mater. 371 (2007) 145-160.

[5] P. Pareige, R. E. Stoller, K. F. Russell and M. K. Miller, Atom probe characterization of the microstructure of nuclear pressure vessel surveillance materials after neutron irradiation and after annealing treatments, J. Nucl. Mater. 249 (1997) 165-174.

[6] T. Toyama, Y. Nagai, Z. Tang, M. Hasegawa, A. Al Mazouzii, E. Van Walle, R. Gerard, Nanostructural evolution in surveillance test specimens of a commercial nuclear reactor pressure vessel studied by three-dimensional atom probe and positron annihilation, Acta Materialia 55 (2007) 6852-6860.

[7] E. Meslin, M. Lambrecht, M. Hérnandez-Mayoral, F. Bergner, L. Malerba, P. Pareige, B. Radiguet, A. Barbu, D. Gómez-Briceno, A. Ulbricht, A. Almazouzi, Characterization of neutron-irradiated ferritic model alloys and a RPV steel from combined APT, SANS, TEM and PAS analyses, J. Nucl. Mater. 406 (2010) 73-83.

[8] P. B. Wells, T. Yamamoto, B. Miller, T. Milot, J. Cole, Y. Wu, J.R. Odette, Evolution of manganesenickelsilicon-dominated phases in highly irradiated reactor pressure vessel steels, Acta Materialia 80 (2014) 205-219.

[9] M. K. Miller, K. A. Powers, R. K. Nanstad, P. Efsing, Atom probe tomography characterizations of high nickel, low copper surveillance RPV welds irradiated to high fluences, J. Nucl. Mater. 437 (2013) 107-115.

[10] K. Lindgren, M. Boåsen. K. Stiller, P. Efsing, M. Thuvander, Evolution of precipitation in reactor pressure vessel steel welds under neutron irradiation, J. Nucl. Mater. 488 (2017) 222-230.

[11] E. Meslin, B. Radiguet, P. Pareige, A. Barbu, Kinetic of solute clustering in neutron irradiated ferritic model alloys and a French pressure vessel steel investigated by atom probe tomography, J. Nucl. Mater. 399 (2010) 137145.

[12] M.J. Konstantinović, G. Bonny, Thermal stability and the structure of vacancysolute clusters in iron alloys, Acta Materialia 85 (2015) 107-111.

[13] B. Minov, M. Lambrecht M, D. Terentyev, C. Domain, M. J. Konstantinović, Structure of nanoscale copper precipitates in neutron-irradiated Fe-Cu-C alloys, Phys. Rev. B 85 (2012) 024202-02420(-6).

[14] K. Verheyen, M. Jardin, A. Almazouzi, Coincidence Doppler broadening spectroscopy in Fe, FeC and FeCu after neutron irradiation, J. Nucl. Mater. 351 (2006) 209-215.

[15] P. Hautojärvi, Positrons in Solids, Topics in Current Physics, Springer, Berlin, vol 12; 1979.

[16] N. Soneda, T. Diaz de la Rubia, Defect production, annealing kinetics and damage evolution in α-Fe: An atomic-scale computer simulation, Phil Mag A 78 (1998) 995-1019.

[17] C. Domain, C. S. Becquart, J. Foct, Ab initio study of foreign interstitial atom (C, N) interactions with intrinsic point defects in α-Fe, Phys. Rev. B 69, (2004) 144112-144112-16.

[18] L. Messina, M. Nastar, T. Garnier, C. Domain, P. Olsson, Exact *ab initio* transport coefficients in bcc Fe-X (X=Cr, Cu, Mn, Ni, P, Si) dilute alloys, Phys. Rev. B 90 (2014) 104203-104203(-15).

[19] G. Bonny, C. Domain, N. Castin, P. Olsson, L. Malerba, The impact of alloying elements on the precipitation stability and kinetics in iron based alloys: An atomistic study, Comp. Mater. Sci. 161 (2019) 309-320.

[20] E. Vincent, C. S. Becquart, C. Domain, Mean field rate theory and object kinetic Monte Carlo: A comparison of kinetic models, J. Nucl. Mater. 382 (2008) 154-159.

[21] Y. Nagai, M. Hasegawa, Z. Tang, A. Hempel, Y. Kawazoe, A. Kawai, F. Kano, Positron confinement in ultrafine embedded particles: Quantum-dot-like state in an Fe-Cu alloy, Phys. Rev. B 61 (2000) 6574-6578.

[22] S. C. Glade, B. D. Wirth, G.R. Odette, P. Asoka-Kumar, Positron annihilation spectroscopy and small angle neutron scattering characterization of nanostructural features in high-nickel model reactor pressure vessel steels, J. Nucl. Mater. 351 (2006) 197-208.

[23] Y. Nagai, Z. Tang, M. Hassegawa, T. Kanai, M. Saneyasu, Irradiation-induced Cu aggregations in Fe: An origin of embrittlement of reactor pressure vessel steels, Phys. Rev. B 63 (2001) 134110-134110(-5).